EUROPEAN ORGANIZATION FOR NUCLEAR RESEARCH
CERN – TS Department

EDMS Nr. 491133

CERN-TS-2004-001 (MME)
CLIC Note 614

New spark-test device for material characterization

M. Kildemo

Abstract

An automated spark test system based on combining field emission and spark measurements, exploiting a discharging capacitor is investigated. In particular, the remaining charge on the capacitor is analytically solved assuming the field emitted current to follow the Fowler Nordheim expression. The latter allows for field emission measurements from pA to A currents, and spark detection by complete discharge of the capacitor. The measurement theory and experiments on Cu and W are discussed.

Paper accepted for publication in Nucl. Instrum. Methods Phys. Res., A (2004)

Geneva, Switzerland
February 2004

1. INTRODUCTION

A large amount of work on electrical breakdown between electrodes in vacuum, has been published in the last 50 years [1-10 and references therein]. There is currently a renewed interest in the subject with respect to the important limitation created by sparking and field emission in future linear colliders [10-15].

The work on a "dc" system presented here, is motivated by the need to increase the understanding of the breakdown process, increase the amount of breakdown data available in order to choose the optimal material, and surface preparation in particular for the irises in the accelerator cavities.

A new measurement scheme, including a larger automation in the data recording, is studied in order to improve the understanding of the breakdown phenomena, and in particular, the relation to material and surface preparation. This paper focuses on the experimental set-up, the measurement theory, and detailed investigation of the recorded data just before and after the spark. The test system and the results appear to be useful for better understanding of the conditioning of accelerator structures and also of field emitter electron guns.

An enlarged statistical and comparative data analysis of the electrical measurements from multiple conditioning series on Cu, Mo, and W, including SEM analysis, will be presented in a separate work [16].

2. EXPERIMENTAL SETUP

The electrodes of the spark-test system have a tip-plane geometry and are located in ultra high vacuum (UHV) at a pressure of less than $3*10^{-9}$ Torr after bake-out. The anode is a mechanically rounded hemispherical tip with diameter 2.4 mm. The fine approach of the tip toward the cathode (sample) is made through a home-made mechanical micro positioning device based on differential levers. The displacement has been calibrated ex-situ and the accuracy of the stage is sub-micrometer when backlash is minimized by correct operation. The sample is a plane electrode mounted on a manipulator stick, which enables lateral displacement to perform sparks at different sites of the same sample. Moreover, for coarse approaching the sample is pushed toward the tip with a second translator stick (electrically insulated from the sample), which has also the effect of reducing mechanical vibrations of the sample. Both the cathode (plane surface) and the anode (hemispherical tip) are chosen of the same material, namely OFHC copper or pure tungsten (99.95 % purity and pinhole free, from Goodfellow) cleaned with the standard CERN cleaning procedure [17] for UHV components.

Fig. 1 shows the schematic layout of the computer controlled spark-test system. It is constituted of the UHV chamber containing the sample and tip, a HV power supply of +/-15 kV (CAEN N570), a home-made switching electronics, a GPIB programmable electrometer (Keithley) and a GPIB programmable oscilloscope (Lecroy) connected to a home-made Rugovsky coil. The electronics, including data acquisition from the electrometer and oscilloscope, is completely controlled by a PC through Labview (National Instruments) real time control software.

The switching electronics, shown more in detail in Fig. 2, is based on computer controlled electro-mechanical relays. The low current switches (all but S2) were designed for 25 kV operation, and were tested before mounting for no leakage (pA) up to 15 kV. The high current switch (S2) is a large hammer type switch (Ross Engineering Corp.,USA), also designed for 25 kV operation.

The system can operate to acquire either field emission current or so called spark-scans. In field emission mode only S4 (Fig. 2) is closed and the electrometer is protected by R_{in} = 10 MΩ by an additional resistor R = 2 MΩ (Fig. 1). The acquisition of a current versus voltage field emission trace takes 0.7 seconds for each point (set high voltage, wait until high voltage reached, and single read-out of current).

In the second type of measurement, called hereafter spark-scan, the electronics operates as follows: The switch S1 (Fig. 2) closes to charge the capacitor C1 at the voltage set on the power supply and opens again. Then the switch S2 exposes the electrodes gap to the high voltage for a set time τ, field emission or a spark may occur and the capacitor is partly discharged. The switch S3 (Fig. 2) is then closed in order to measure the remaining charge on the capacitor, by discharging it completely through a current divider and an electrometer. After this cycle a new cycle can start with a higher voltage. The total time for each measurement point in this mode is 12 seconds (2 s for loading C1, 2 s exposure, 2-4 s for measurement read out and initialisation of the electrometer, setting of new high voltage, and some additional time to avoid timing errors). The selected time of exposure of the gap to high voltage, τ = 2 s, allows us to use millisecond range high-voltage electromechanical relay switches. Finally the result of the spark-scan is the field resulting in the gap after the time τ as a function of the field given by the charged capacitor.

The breakdown current is limited by a 27 Ω resistance, in order to improve the control of the transient response occurring upon switching on the high voltage across the gap. Similarly, the voltage overshoot, which would occur by abrupt connection of the capacitor to the gap is reduced by keeping S5 (Fig. 2) closed for operation in this mode (C2 = 1 nF). The main capacitor is chosen as C1 = 28 nF so that with typical voltages at spark from 6-12 kV there is an available energy of 0.5-2 J and maximal sparking currents of about 200-400 A.

3. THEORETICAL BACKGROUND

Field emission sites are known to be possible precursors of electrical breakdown [2]. The field emission properties of an electrode gap are normally described for simplicity by the Fowler-Nordheim (FN), Eq. (1-6, 10,11, 18).

$$I[A] = A_e \frac{1.54x10^6 \beta^2 E^2 [MV/m]}{\phi[eV]} e^{10.41\phi^{-1/2}} e^{-\frac{6.53x10^3 \phi^{3/2}}{\beta E}} \equiv \xi E^2 e^{-\gamma/E} \qquad (1)$$

where the field emission current (I) is measured in A, the electric field (E) in MV/m, the emission area (A_e) in m^2, the work function (ϕ) in eV. β is a dimensionless constant known as the field enhancement factor. Finally, γ and ξ are constants including material properties and gap geometry. In particular

$$\beta = \frac{6.53x10^3 \phi^{3/2}}{\gamma}$$

which defines directly the local field where the field emission occurs as $E_{loc} = \beta E$. Temperature corrections [18] and space charge limitations [19,20] to field emission currents are here neglected. For the interpretation FN logarithmic plots of Eq. (1) are commonly used:

$$\ln\left(\frac{I}{E^2}\right) = \ln(\xi) - \frac{\gamma}{E} \qquad (2)$$

In practice, the usual field emission measurement cannot be performed for parameters close to breakdown (high fields and high currents), since the electrometer needs to be protected by a large series resistance. In the present approach by measuring the charge remaining on the capacitor one can measure at increasing voltages up to the spark and above it and at the same time keep field emission information, although integrated over the discharging time τ. The possibilities offered by this alternative approach are investigated in detail in the following paragraphs.

In the case of the discharging capacitor in field emission mode, the field-emitted current equals the loss of charge on the capacitor:

$$\frac{dQ}{dt} = -I(t) = -\xi E^2 \exp(-\gamma / E) \tag{3}$$

Let us define the field on the gap resulting from the remaining charge on the capacitor at time t after closing of switch S2:

$$E(t) = \frac{Q(t)}{C_1 d} \tag{4}$$

where d is the distance between the tip and plane in the gap and the approximation for flat parallel electrodes is used for calculating the field as V/d. Calculations performed with the method of image charges on a sphere-plane geometry to simulate the tip-sample configuration demonstrate that the field on the surface plane remains higher than 80 % of V/d within a lateral radius (r) of 100 µm, and falls off to 50 % at approximately r = 150 µm. Using the sphere plane geometry will obviously involve some average field within the electric field profile. Eq. (3) is then rewritten for simplicity giving the following differential equation

$$E' = -\hat{\xi} E^2 \exp(-\gamma / E) \tag{5}$$

where ξ is normalized as $\hat{\xi} = \frac{\xi}{Cd}$. Eq. (5) was solved in this work (the author is unaware of previous solutions to this equation), and happened to have the simple analytical solution:

$$\frac{(E_i - E_\tau)}{E_i E_\tau} = \frac{\ln\left\{1 + \hat{\xi}\gamma\tau \exp(-\gamma / E_i)\right\}}{\gamma} = \frac{\ln\left\{1 + \frac{\gamma\tau I_i}{CdE_i^2})\right\}}{\gamma} \equiv \eta, \tag{6}$$

or solved with respect to the current:

$$I_i = \frac{CdE_i^2}{\tau\gamma}\left(\exp\left(\gamma\frac{(E_i - E_\tau)}{E_i E_\tau}\right) - 1\right) \tag{7}$$

where τ is the time available for discharging the capacitor connected to the gap, E_i is the initial field at t = 0, E_τ is the remaining field at time τ, and I_i is the field emission current from Eq. (1) at time t = 0. Eq. (7) shows that the initial field emission current I_i can be estimated from the quantities E_i and E_τ and thus the currents can be estimated from spark scan measurements. This gives access to the evaluation of extremely high field emission currents, without the need of any protection resistor, i.e. the condition for studying electrical breakdown.

Since the γ value can only be determined from standard FN plots it is useful to look for suitable expansions of Eq. (6), which can reveal the material properties. Let $x = \xi\gamma\tau \exp(-\gamma/E)$. Two expansions, for low and high field emission currents can be performed, respectively. At low currents, $0 < x \leq 1$ or equivalently $I_i << CdE_i^2/(\gamma\tau)$, the development of the logarithm gives $ln(1+x) \approx x$. Inserting this in Eq. (6) and taking the logarithm becomes:

$$\ln\left[\frac{(E_i - E(t))}{E_i E(t)}\right] \approx \ln(\xi t) - \gamma / E_i \tag{8}$$

which is similar to the standard FN plots for field emission current measurements (Eq. (2)). Eq. (8) has a limited range of validity with very small currents or high charges remaining on the capacitor after τ. At such small currents, however, the capacitor method does not have a sensitivity comparable to standard field emission measurements and the method proposed by Eq. (8) is not further discussed in this paper. Determination of initial Fowler Nordheim type parameters, is therefore performed according to traditional field emission measurements (Eq. (1) and (2)).

At high currents x >> 1 or equivalently

$$I_i >> \frac{CdE_i^2}{\gamma\tau},$$

the discharging behaviour of the capacitor quickly moves into an asymptotic solution and Eq. (6) reduces to

$$\frac{(E_i - E_\tau)}{E_i E_\tau} \approx \frac{\ln\{\xi\gamma\tau\}}{\gamma} - \frac{1}{E_i} \tag{9}$$

Solving this equation for E_τ it results that its asymptotic limit does not depend on E_i, giving:

$$E_\tau = \frac{\gamma}{\ln(\xi\gamma\tau)} \tag{10}$$

The condition

$$I_i >> \frac{CdE_i^2}{\gamma\tau}$$

is matched for currents of the order of μA in the present set-up and Eq. (13) appears thus as the most suitable form for monitoring of the material properties under electric fields approaching the sparking event. Let us therefore rewrite Eq. (6) in a suitable form similar to Eq. (10):

$$E(\tau) = \frac{E_i}{E_i\eta + 1} \tag{11}$$

Eq. (11) shows clearly that for negligible field emission ($\eta \approx 0$) $E(\tau)$ will be identical to E_i, while for larger field emission then $E(\tau)$ will deviate from E_i, and rapidly move towards the asymptotic solution of Eq. (10).

Let us study in detail the variation in the E_τ, as a function of modifications of the field emission area A_e , the field emission enhancement factor β and the work function ϕ, all included in γ and ξ. For this it is useful to consider a first order development of Eq. (10) around a point (ξ_0, γ_0) which in practice can be found from field emission measurements. A Taylor expansion around the operating point for

$$\left(\frac{\Delta\xi}{\xi_0},\frac{\Delta\gamma}{\gamma_0}\right)<<1 \quad \text{gives:} \quad E_{\tau x>>1}\approx\frac{\gamma_0}{\ln(\hat{\xi}_0\tau\gamma_0)}\left\{1+\frac{\Delta\gamma}{\gamma_0}-\frac{\Delta\gamma}{\gamma_0\ln(\hat{\xi}_0\tau\gamma_0)}-\frac{\Delta\hat{\xi}}{\hat{\xi}_0\ln(\hat{\xi}_0\tau\gamma_0)}\right\},$$

which shows that E_τ is mainly sensitive to the exponential factor γ. Further, by using that

$$\frac{\Delta\gamma}{\gamma_0}\approx-\frac{\Delta\beta}{\beta_0}+\frac{3\Delta\phi}{2\phi_0}, \text{ and } \frac{\Delta\hat{\xi}}{\hat{\xi}_0}\approx\left(\frac{2\Delta\beta}{\beta_0}+\frac{\Delta A_e}{A_e}-\frac{\Delta\phi}{\phi_0^{3/2}}\left(\sqrt{\phi}+5.205\right)\right),$$

we get

$$E_{\tau x>>1}\approx\frac{\gamma_0}{\ln(\hat{\xi}_0\tau\gamma_0)}\left\{1-\frac{\Delta\beta}{\beta_0}\left[1+\frac{3}{\ln\left(\hat{\xi}_0\gamma_0\tau\right)}\right]-\frac{\Delta A_e}{A_{e0}\ln(\hat{\xi}_0\tau\gamma_0)}+\frac{\Delta\phi}{\phi_0^{3/2}}\left(\sqrt{\phi_0}\left(\frac{3}{2}-\frac{1}{2\ln(\hat{\xi}_0\tau\gamma_0)}\right)+\frac{5.205}{\ln(\hat{\xi}_0\tau\gamma_0)}\right)\right\} \tag{12}$$

The factor $\ln(\hat{\xi}_0\tau\gamma_0)$ is typically of the order of 13, and Eq. (12) may for clarity be simplified as

$$E_{\tau x>>1}\approx\frac{\gamma_0}{\ln(\hat{\xi}_0\tau\gamma_0)}\left\{1-1.23\frac{\Delta\beta}{\beta_0}+1.65\frac{\Delta\phi}{\phi_0}-\frac{\Delta A_e}{13A_{e0}}\right\} \tag{13}$$

Hence, in the asymptotic region, Eq. (13) shows that E_τ decreases for higher field enhancement (β), increasing field emission area (A_e) and decreasing work function. Similarly, E_τ increases with both decreasing β and decreasing A_e, while E_τ increases with higher work function. Furthermore, Eq. (13) shows that E_τ in the asymptotic region is an order less sensitive to changes in A_e compared to changes in work function or the field enhancement factor.

The E_τ calculated from the numerical/analytical solution, i.e. Eq. (5) and (6), is shown in Fig. 3, as a function of the initially applied electric field E_i. The dotted lines give the asymptotic solution as in Eq. (10). The values used in the simulations were, C = 28 nF, d = 20 μm, β = 30, $A_e = \pi r^2_e$ (r_e = 20 nm) and ϕ = 4.5 eV. The Fig. 3 also shows the results of E_τ, for the perturbed solutions, by changing only one parameter at a time (e.g. β from 30 to 35). The changes are in good correspondence with the results of Eq. (13). It is observed from Fig. 3 that in the asymptotic region a 17 % increase in β gives about a 20 % decrease in E_τ. Similarly, an 11 % increase in ϕ gives an 18 % increase in E_τ. However, an increase of half an order of magnitude in the emission area gives only a 6 % change in E_τ. This simulation is thus in good correspondence with the behaviour described by the approximations (12) and (13).

4. RESULTS AND DISCUSSION

In order to demonstrate the results that can be obtained from the automated spark test system, a set of measurements on copper and tungsten are presented. The evolution of the behaviour with respect to breakdown as a function of the number of spark-scans (conditioning) is discussed.

A selected number of spark-scans, or E_τ as a function of E_i curves, measured at the same site on copper are shown in Fig. 4. By taking for instance the curve labelled S22 it appears that the general form is in agreement with the simulated curves (Fig. 3). E_τ rises initially as E_i, while it deviates upon reaching the onset of field emission, since the field emission current discharges the capacitor during the time τ and the remaining field E_τ is therefore lower than E_i. Then E_τ rapidly saturates towards the asymptotic solution given by Eq. (10). Upon the spark, E_τ drops to zero, since the capacitor is totally discharged in the spark. The spark is accompanied by a current pulse, which is induced in the Rugovsky coil and is acquired by the oscilloscope. The occurrence and the shape of the acquired pulse enables it to be insured that the capacitor has been discharged through a spark event and excludes any effects of leakage currents on other sites of the instrumentation. The value of E_i at which the first spark occurs along a spark-scan is defined as the first breakdown field E_{b1}. Many spark-scans are shown in Fig. 4 and all the traces are denoted by the spark history (number of sparks), i.e. the curve denoted S16, correspond to the curve prior to the 16th spark.

In order to characterize the field emitting properties at the beginning of the spark-scan the field emission current as a function of applied field is measured and the corresponding FN plots traced. The FN plots related to the spark scans in Fig. 4 are presented in Fig. 5. First of all it is noted that the curves with lower slope, i.e. γ smaller or higher β values (Fig. 5), correspond to the lower asymptotic E_τ value in Fig. 4, as expected from Eq. (10). The work function is strongly correlated with the β value. From the curves in Fig. 5 the prefactor ξ and exponential factor γ can be extracted directly (Eq. (2)) and the field enhancement factor β can be calculated for a given value of the work function. In the quantitative analysis, the surface work function changes are neglected and a value of ϕ is fixed at ϕ = 4.5 eV corresponding approximately to the average value for metallic (polycrystalline) Cu [21]. The standard conditioning curves [3,9] for the same series of spark-scans for copper, are shown in Fig. 6, where both the evolution of the first breakdown field (E_{b1}) and the field enhancement factor (β) as a function of the number of sparks are displayed. The curve shows continuous oscillations without any clear decrease of the average β or increase of the average E_{b1}, so that no clear conditioning effect can be visible.

To demonstrate the consistency of the system operating in spark-scan mode and field emission current mode it is useful to compare the results for I_i from both measurements by introducing in Eq. (7) the parameters extracted from the FN curves. The results are shown in Fig. 8 from the series of data on Cu. Indeed, Fig. 8 shows an overlap at field-emitted currents of the order of μA. The discharging capacitor method also allows changes or deviations in the field emitted current from the standard FN emission regime to be observed.

The local field at the field emission site and hence at the site with highest field in the gap, E_{loc}, can be calculated multiplying β*E_{B1} and using the β extracted from FN curves. This field at breakdown is also commonly denoted critical breakdown electric field [22]. Fig. 7 illustrates the evolution of the local field estimated in this way as a function of the number of sparks. The local field E_{loc} quickly approaches an average value of 10100 MV/m compared to literature values around 5000-7000 MV/m (6500 MV/m [1, 6, 22]). It should be noted in this case that for the present calculated β value and hence E_{loc} the work function value has been fixed at 4.5 eV [21] and variations of 1 eV generate fluctuations of 33 % in the estimated local field in the

sense that a lower ϕ would give a lower E_{loc}. Such variations are likely to occur after a few sparks on the same spot due for instance to cleaning of the surface from the airborne contamination, removal of the oxide for the oxidised state, melting through electron stimulated desorption and heating. It is uncertain at the moment how much the latter effects change the work function. In case of adsorbates, then CH_n are commonly known to considerably lower the work function (due to charge transfer), while e.g. atomic oxygen has a tendency to increase the work function [21], with some dependency on the crystal face [21]. The estimated local field is also sensitive to geometrical changes of the emission spot during the spark scan, i.e. modifications of the initially determined β value may occur just prior to the breakdown.

Let us now inspect in more detail the evolution of the spark-scans as a function of their number as presented in Fig. 4. It is noted that the initial behaviour described here is found systematically on many similar curves recorded from different conditioning series at different points on the same copper sample. The first scan (S1), shows that the breakdown takes place before E_τ reaches the asymptotic level. By using Eq. (7) the field emitted current is estimated to be only 0.6 μA at E_{b1}. It is observed that the breakdown field E_{b1} equals about the average value, while the local field (Fig. 7) appears low compared to most of the other sparks in the series. The as-received surface consists of adsorbates on native copper oxide and further sparks at the same site are expected to partially remove the oxide [22]. The scan labelled S4 indicates that the surface can now hold a much higher electric field E_{b1} (Fig. 6). At the same time also β has apparently increased (Fig. 6), which seems contradictory, since a high β gives a higher local field and hence is expected to give a worse behaviour against breakdown. The apparent contradiction could indicate that the assumption of a constant work function is no longer valid. By inspecting the trend from several conditioning spark scans (not shown here), it appears likely that the work function is in most cases initially lower for the adsorbate/oxide/Cu state. Both the work function and the first breakdown field, appears generally to increase with the first few sparks, which is the case if one assumes that the effective work function in the clean oxidised state is considerably larger than both the clean metal surface and the adsorbate/oxide/Cu work function. The work function finally approaches the average (polycrystalline) copper value as the oxide is removed. The scan S4 appears to be in the intermediate region between the oxidised and the clean state. Such details can only be investigated by in situ surface analysis techniques with sufficiently high spatial resolution [9], and possibly by applying lower stored energies on the capacitor. In spite of possible chemical modifications the behaviour of the current always satisfies the FN behaviour described by Eq. (1), as it can be seen from the linearity in Fig. 5. After several spark-scans the curves denoted S9-S16 indicate that the capability of the surface to withstand breakdown gets worse again: E_{b1} decreases and the values of β increase. An alternate sequence of worsening (S19-S22) and improvements (S9-S16 and after S22) continues with evident correlation between the behaviour of E_{b1} and β. Since the surface is likely to be cleaned from the native oxide and adsorbates after a few sparks, such cycles are probably due to topographic modifications (local melting, formation of craters, droplets and tips), so that a configuration stable against breakdown cannot be reached for fields above 220-250 MV/m. The estimated field emitted currents (Eq. (9)) reach almost 4 mA at S22, which is the maximum found for the copper surface investigated in the present study.

The main aim of the developed spark-test system is the possibility to perform diagnostics on different materials with respect to breakdown behaviour. In order to demonstrate that the difference between materials can be revealed a similar study has been performed on tungsten.

Fig. 9 shows some selected E_τ scans during the conditioning series, which are presented using the same notation as for the copper series above. The corresponding standard conditioning curves with the evolution of E_{b1} and β for the same series are shown in Fig. 10 and 11 showing the evolution of the estimated local field. The most striking difference between Cu and W is the way that E_{b1} for W increases almost monotonically as a function of the number of sparks and reaches breakdown fields of about 500 MV/m compared to 220-250 MV/m for Cu. Moreover, the field enhancement factor β appears to decrease (Fig. 10) as a function of number of sparks, except for occasional spikes and stabilizes at much lower values than for copper (Fig. 5). Similarly the maximal estimated field emission currents just prior to breakdown increase from some mA (S3) up to tens or hundreds of mA (S16, S25), for the conditioned surface.

A peculiar feature is observed in the spark-scans in Fig. 9, which was less pronounced on copper, namely the drop in E_τ (most of the curves in Fig. 9) as a function of E_i just after reaching the asymptotic limit (flat part). Two possible explanations are conceivable. On the one hand this could be ascribed to a modification in the field emission parameters, i.e. lowering of the work function, increase of β, or increasing emission area (see Eq. (13)) during the spark-scan. On the other hand, the systematic occurrence and the gradual change could be a fingerprint of the onset of thermionic field emission. This would be due to the Joule heating of the emitter when higher and higher field emission currents are flowing. Using the estimated emission areas (from the Fowler Nordheim log plots), the current densities in the conditioned state are here estimated to be in the range 10^6 to 10^9 A/cm^2, which is sufficient for the onset of thermionic emission and in some cases probably sufficient for space charge limited field emission. Such a change of the emission mechanism, which becomes a complex nonlinear problem through the Joule heating of the emission spot, but can be accounted for with a temperature dependent prefactor in a restricted range of temperature and field [18]. The values given in Fig. 9 for the current are thus only estimations. One may speculate that the observed difference in the E_τ characteristics in the asymptotic region between W and Cu, could be a result of the higher heat conductivity of Cu compared to W. In terms of the latter interpretation, Fig. (4) suggests that in case of Cu, breakdown will take place before thermionic field emission starts dominating. Furthermore, (9) and (10), show that the W surface appears not to rupture in a catastrophic way, such as was the case for Cu, before extremely high fields (close to 650 MV/m) are applied.

The local fields in the conditioning scan for W (see Fig. 11), show a much more gradual increase (hardening) compared to the case of Cu (Fig. 7). There appears also to be a much larger scattering in the local field values for W, both to lower values, and to unrealistically higher values (S19, S26…) as previously reported, particularly in case of W [22]. Examples of such changes are given by the initially large β value in S19 and S26 in Fig. 10, resulting in unrealistic high local field values. The corresponding spark scans S19 and S26 are shown in Fig. 12, where E_τ first drops abruptly around 200 MV/m (arrow A), and then gradually increases as a function of E_i (arrow B). Space charge effects can also play a relevant role. It is plausible from the estimated current densities, that thermionic field emission sets in at (A), and that the ramp (B) is due to space charge limited field emission. A process strongly correlated to thermionic emission and even space charge emission, is the possibility of recession or dulling/blunting of the field emitter tip due to surface migration [1, 23] activated by Joule heating. These are issues which are to be verified by further studies, i.e. by two consecutive spark scans ending before the sparking event. Thermionic and space charge limited emission alone should make two consecutive scans identical, while a blunting or a change in field emitter parameters should result in completely different spark scans.

For some of the lower lying values in the estimated local field in Fig. 11, such as S25 and S16, we find a field emitting current with increasing field which is larger than expected from Fowler Nordheim emission. For such curves there is no simple relation between the local and the applied field. In this case only the spark scan method developed and presented here allows following the behaviour of the gap as a function of the applied field up to the breakdown and enables the monitoring of the deviation from FN behaviour of the current. Such an effect cannot be observed by the usual FN measurements, when only recorded over a lower range of currents.

All the measurements related to the field emission give direct information about the state of the cathode, however, the capability to withstand breakdown may also partly be triggered by the anode. In the present experiment this was the main reason to choose always the same material for both electrodes. In fact the field emission behaviour is important also for the effects on the anode, since it results in electron bombardment of the anode surface and hence heating and electron stimulated desorption. The discussion on whether the electron bombardement in pre-breakdown field emission is sufficient to cause evaporation and trigger the vacuum breakdown (see e.g. [1, 2, 3]) is out of the scope of this report.

5. SUMMARY AND CONCLUSIONS

A computer controlled spark test system has been developed, analysed and tested. The system is based on discharging a capacitor on the electrode gap in combination with computer controlled high voltage switching and charge measurements. The analytical expression derived for the remaining charge on the capacitor due to discharging through field emission only is applied to better understand the phenomena leading to breakdown. It enables to relate the high current and the low current regime, where field emission currents are much too high for standard field emission current measurements. The capabilities of the spark test system are illustrated through the measurements on copper and tungsten samples. The conditioning behaviour of both materials is investigated with respect to breakdown field and field enhancement factor β as a function of the number of sparks by measuring a series of spark scans. The correlation along the conditioning behaviour between field emission (β parameter) and the breakdown field observed for tungsten and copper demonstrates the validity of the analysis through field emission combined with spark scan measurements. The system is able to reveal the differences between the materials and can therefore be used as a diagnostic tool to select materials with respect to breakdown resistance. Literature results are reproduced and as a new feature the evolution of the field emission current behaviour as a function of the applied field can be followed up to high currents close to the breakdown condition.

ACKNOWLEDGEMENTS

The author acknowledges particularly help and discussions with M. Taborelli and S. Calatroni. Furthermore, help with the UHV system from W. Vollenberg and H. Neupert, and general discussions with C. Benvenuti and W. Wuensch are acknowledged.

REFERENCES

1. P.A. Chatterton, " Vacuum Breakdown," in *Electrical Breakdown in gases*, J. M. Meek and J.D. Craggs eds. (Wiley,1978).
2. R.V. Latham (ed.), "High Voltage Vacuum Insulation," (Academic Press, 1995).
3. G.A. Mesyats and D.I. Proskurovsky, *Pulsed Electrical Discharge in Vacuum* (Springer, 1989).
4. J.M. Lafferty (ed.) *Vacuum arcs,* (Springer,1987).
5. Y.P. Raizer, *Gas Discharge Physics* (Springer, 1987).
6. D. Alpert, D.A. Lee, E.M. Lyman, and H.E. Tomaschke, "Initiation of electrical breakdown in ultrahigh vacuum," Surf. Sci. (1964) 35-49.
7. D.I. Proskurovsky and A.V. Batrakov, "Treatment of the electrode surfaces with intense charged-particle flows as a new method for improvement of the vacuum insulation," in *proceedings of international symposium on discharges and electrical insulation in vacuum*, **1** (2000, China) 9-16.
8. D.I. Proskurovsky, in *proceedings of international symposium on discharges and electrical insulation in vacuum*, **1** (2002, France) 47-153.
9. S. Kobayahsi, K. Sekikawa, K. Asano and Y. Saito, " Surface conditions and electrical breakdown characteristics of ozonized water treated copper electrodes of a vacuum gap," in *proceedings of international symposium on discharges and electrical insulation in vacuum*, **1** (2000, China) 47-50.
10. H. Padamsee, J. Knobloch and T. Hays, *RF Superconductivity for accelerators* (Wiley, 1998). Chapters 10, 11 and 12.
11. J.W. Wang and G.A. Loew, "Field emission and RF-breakdown in High-Gradient room temperature Linac Structures," SLAC-PUB-7684 (1997).
12. G.A. Loew and J.W. Wang, "RF breakdown in room temperature electron LINAC structures," (1988) SLAC-PUB-4647.
13. J.W. Wang and G.A. Loew, "RF breakdown in Copper electron room temperature LINAC structures," (1988) SLAC-PUB-4866.
14. P.B. Wilson, "A plasma model for rf breakdown in accelerating structures," SLAC-PUB-8653 (2000).
15. W. Wuensch, "CLIC 30 GHz accelerating structures development," CLIC-NOTE 569 (2003).
16. C. Benvenuti, S. Calatroni, J.M. Dalin, S. Doerbert, M. Kildemo, M. Taborelli, W. Wuensch, "Automated spark testing, used to study Mo, W and Cu with application to linear colliders," To be submitted to Nucl. Meth. and Instr. (2003).
17. N. Hilleret, C. Scheuerlein, M. Taborelli, "The secondary-electron yield of air-exposed metal surfaces," Appl. Phys. A **76** (2003) 1085-1091.
18. E.I. Murphy and R.H. Good, Jr, , "Thermionic emission, field emission and the transition region," Phys. Rev. 102 (1956) 1464-1472.
19. J.P. Barbour, W.W. Dolan, J.K. Trolan, E. E. Martin, and W. P. Dyke, " Space-Charge Effects in Field emission," Phys. Rev. **92** (1953).
20. W.A. Anderson, "Role of space charge in field emission cathodes," J. Vac. Sci. Technol. B **11** (1993) 383-386.
21. J. Holzl, F.K. Schulte and H. Wagner, "work function of metals," in *Solid Surface Physics* (Springer,1979).
22. B.M. Cox, "Variation of the critical breakdown field between copper electrodes in vacuo," J. Phys. D. Appl. Phys., **7** (1974) 143-151.
23. W.P. Dyke, F.M. Charbonnier, R. W. Strayer, R.L. Floyd, J.B. Barbour and J.K. Trolan, "Electrical stability and life of the heated field emission cathode," J. Appl. Phys. **31** (1960) 790-805.

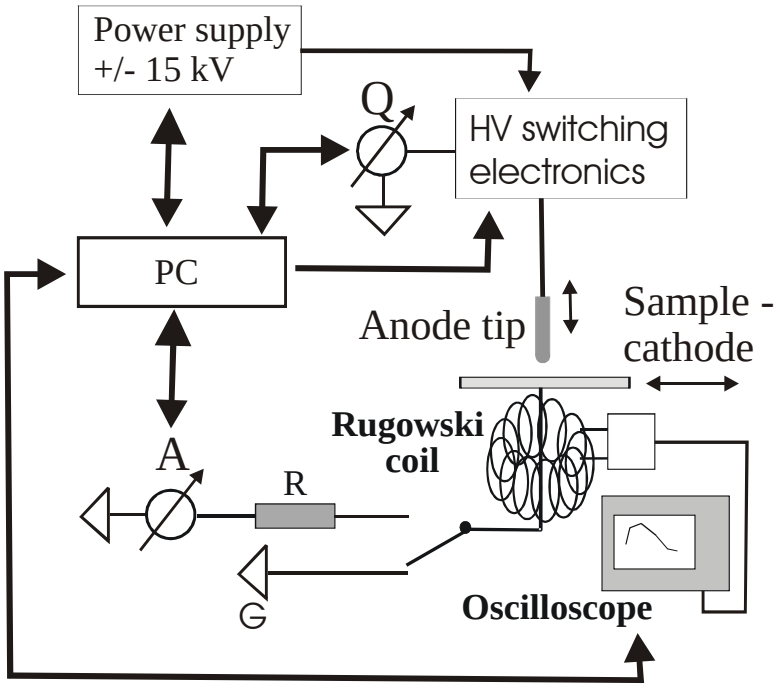

Fig. 1: Schematic layout of the automated spark system

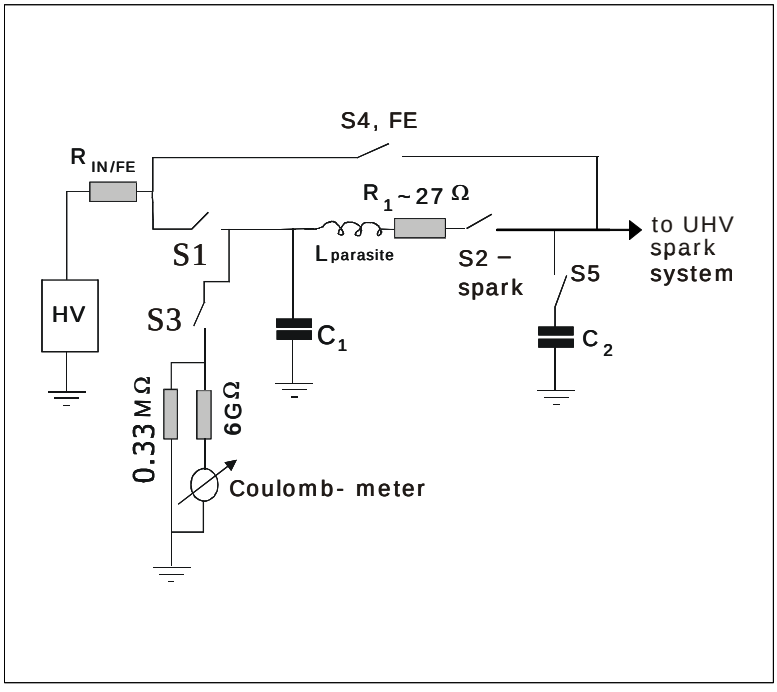

Fig. 2: Details of the switching electronics for combined field emission and spark test measurements.

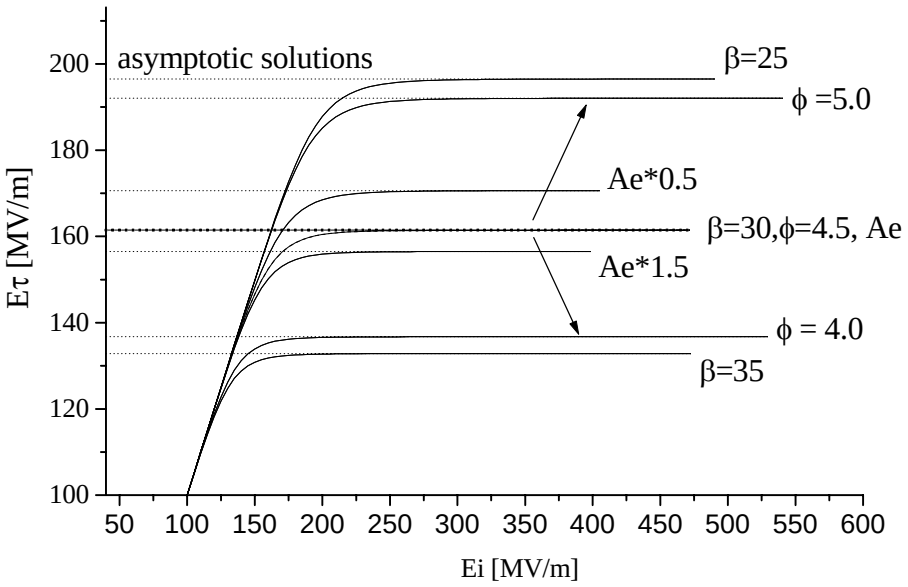

Fig. 3: Simulated E_τ as a function of E_i, using the numerical solution and the asymptotic solution (dotted horizontal lines) of Eq. (10). The middle curve shows the unperturbed solution (open squares) with β_0=30, ϕ_0=4.5 eV and A_{e0} = $\pi^* r_{e0}^2$ (r_{e0}=20 nm). The surrounding curves (full lines) show the variation in E_τ for the indicated changes in the field emission parameters.

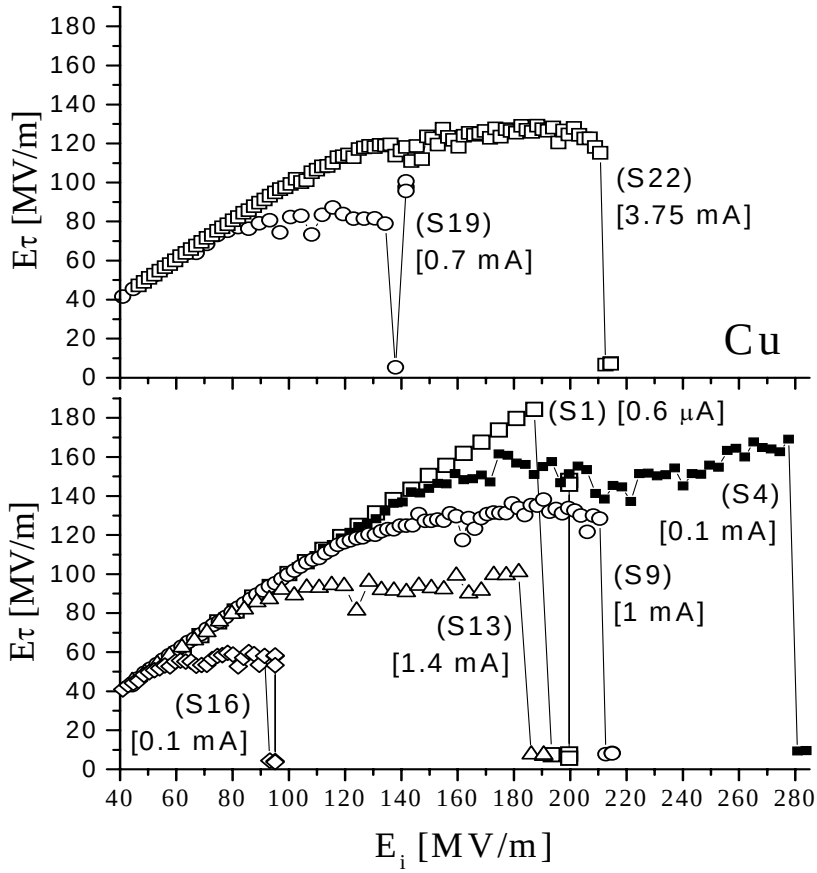

Fig. 4: Selected spark scans of E_τ as a function of applied initial field (*Ei*) recorded in a single conditioning series on Cu. The curves are denoted by S_j, where j is the following spark number. The figure also gives the estimated field emission currents using eq. (7).

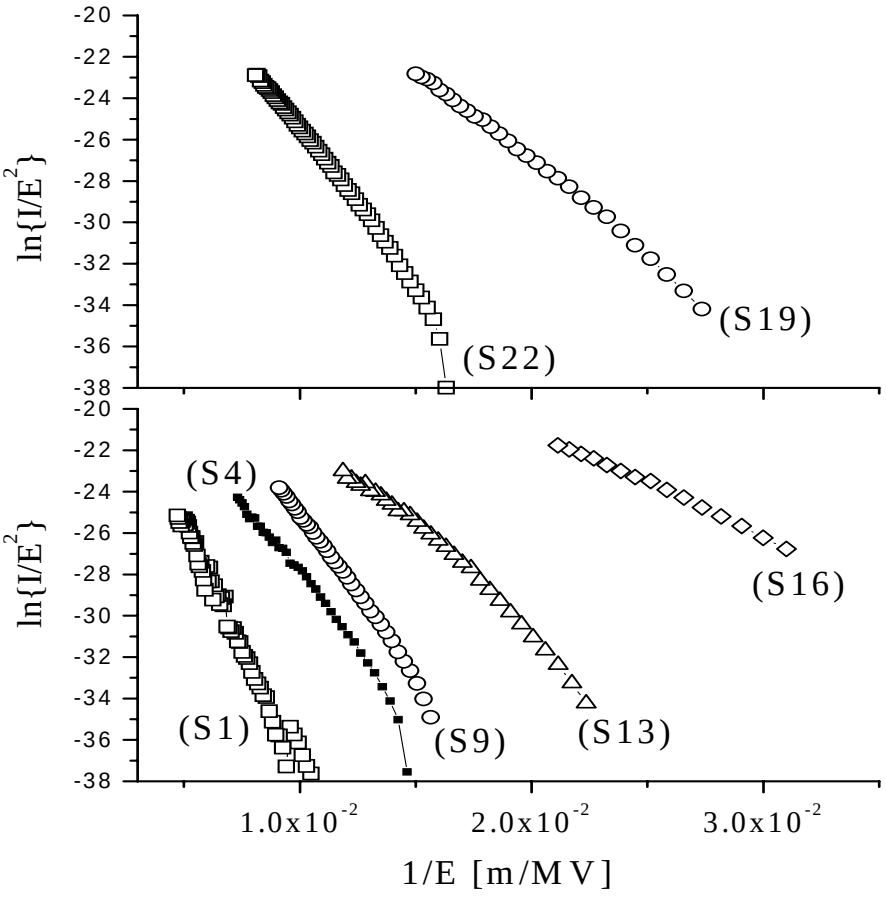

Fig. 5: The standard Fowler Nordheim plots recorded prior to the spark scans, corresponding to Fig. 4.

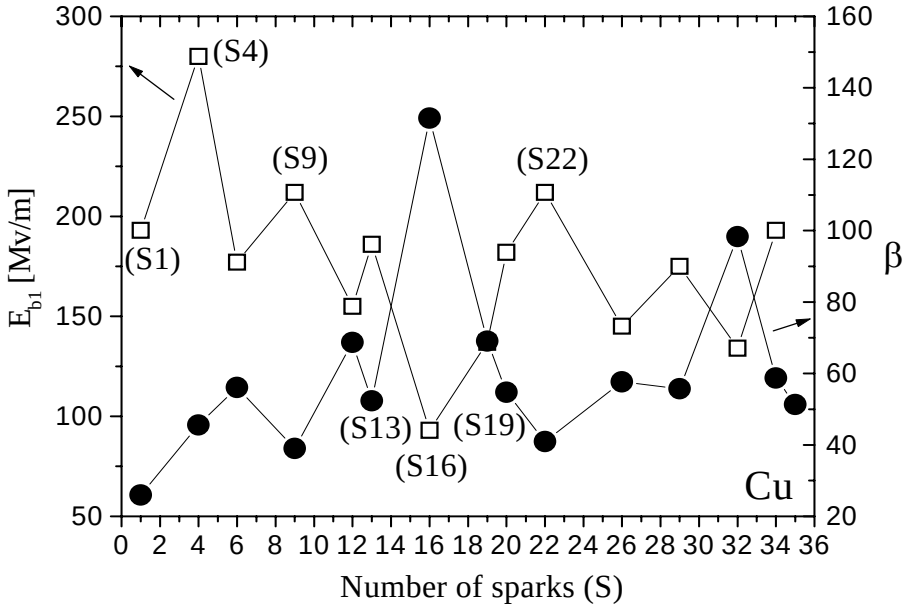

Fig. 6: Conditioning curves for Cu. The figure shows the first breakdown fields (E_{b1}) (open squares, left axis), and the field enhancement factor (β) (full circles, right axis), as a function of number of sparks.

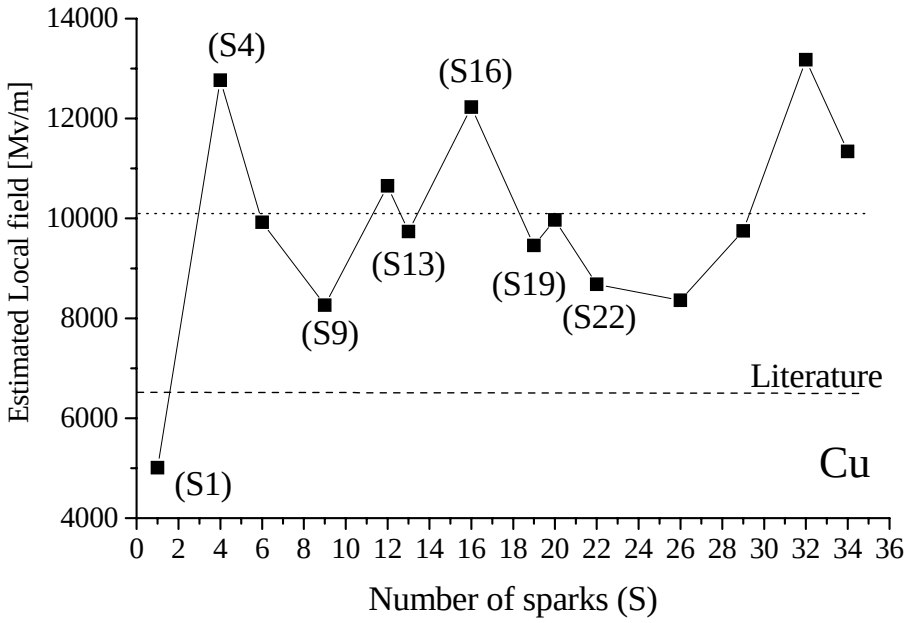

Fig. 7: The variation of the estimated local field defined as $E_{loc} = \beta^* E_{b1}$, as a function of number of sparks, for the data recorded on Cu.

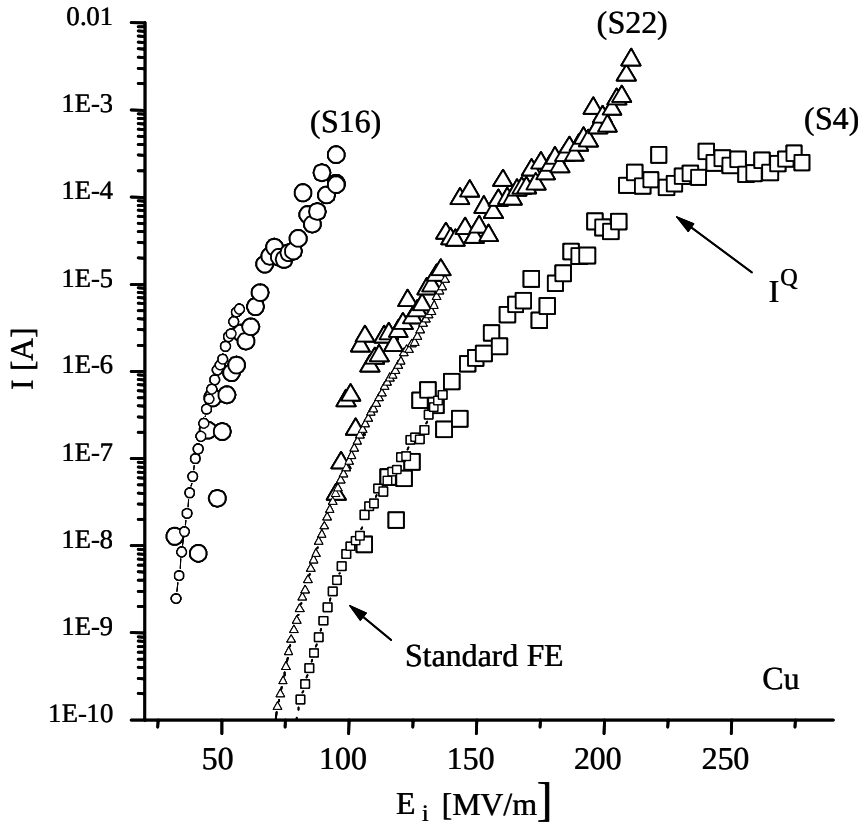

Fig. 8: The recorded field emission current I[A] (small symbols), and the field emission current I_i estimated from the E_τ scans using Eq. (7) (large symbols).

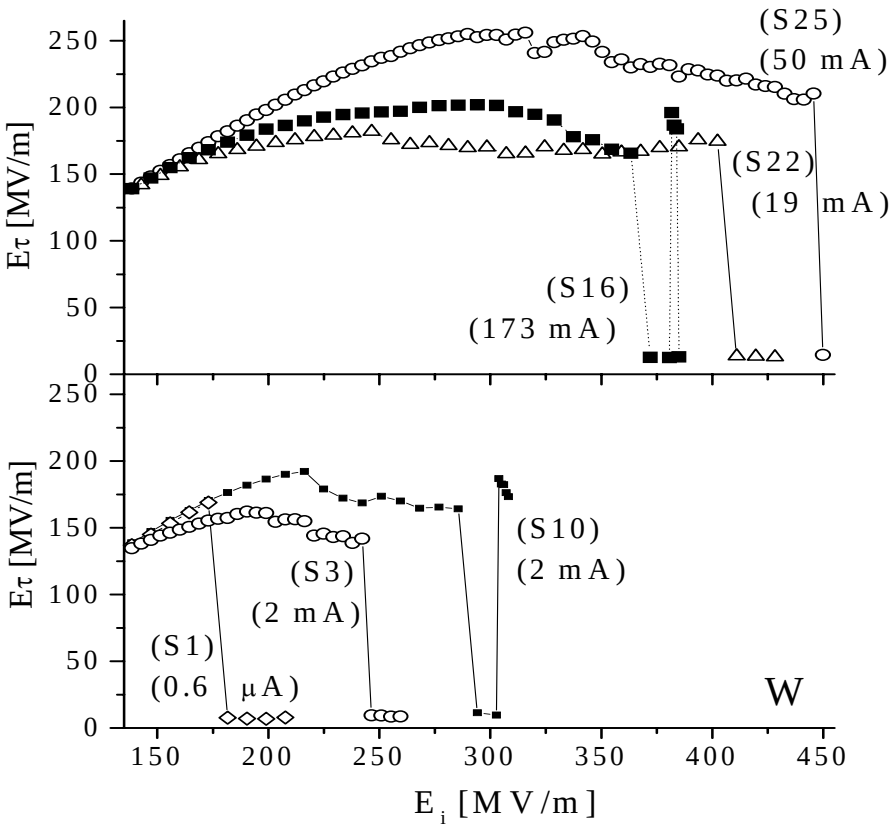

Fig. 9: Selected spark scans of E_τ as a function of applied initial field (E_i) recorded in a single conditioning series on W.

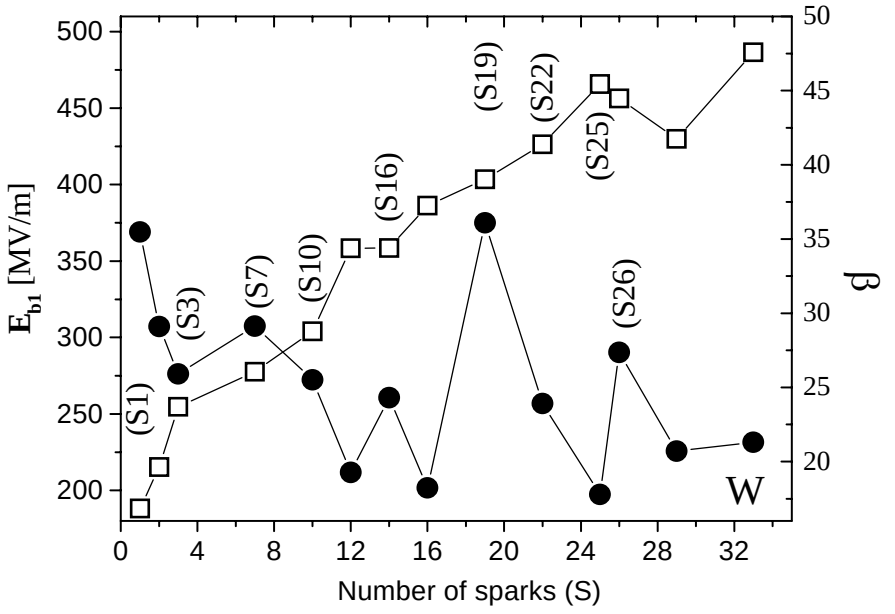

Fig. 10: Conditioning curves for W. The figure shows the first breakdown fields (E_{b1}) (open squares, left axis), and the field enhancement factor (β) (full circles, right axis), as a function of number of sparks.

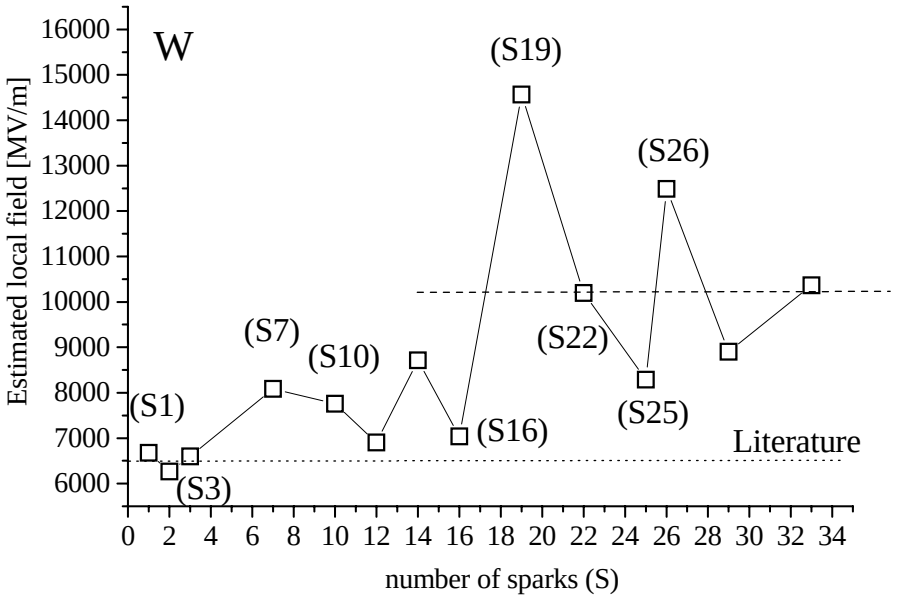

Fig. 11: The variation of the estimated local fields defined as $E_{loc} = \beta^* E_{b1}$, as a function of number of sparks, for the data recorded on Cu.

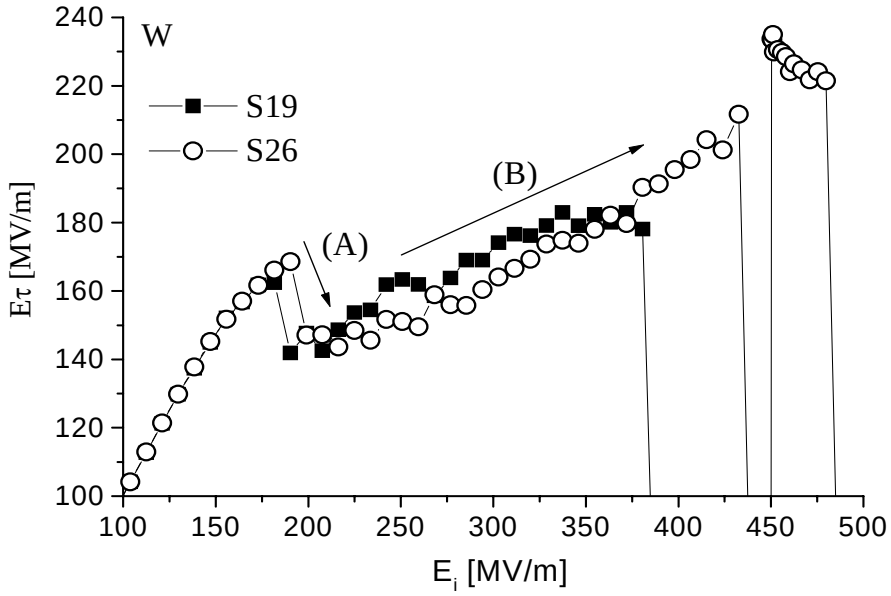

Fig. 12: The spark scans of E_τ on W, for S19 (full squares) and S26 (open circles), corresponding to Fig. 10 and 11. The arrows denoted (A) and (B) indicate deviations from standard FN emission.